Journal of Materials Chemistry A

PAPER

View Article Online
View Journal | View Issue

Cite this: J. Mater. Chem. A, 2014, 2, 13541

Controllable growth of high-quality metal oxide/conducting polymer hierarchical nanoarrays with outstanding electrochromic properties and solar-heat shielding ability†

Dongyun Ma,[ad] Guoying Shi,[c] Hongzhi Wang,*[a] Qinghong Zhang[b] and Yaogang Li*[b]

Received 9th April 2014
Accepted 10th June 2014

DOI: 10.1039/c4ta01722f

www.rsc.org/MaterialsA

The high performance of organic/inorganic hybrid materials relies largely on a scrupulous design of nanoarchitectures so that the organic and inorganic phases can work synergistically. We present a powerful two-step solution-based method for the fabrication of hierarchical metal oxide/conducting polymer heterostructured nanoarrays. Demonstrated examples include different nanostructures (nanorod arrays, nanorod-based networks and nanoplate arrays) of metal oxides (WO_3 and NiO) and PANI (nanostubs, nanoparticles and nano-wrinkles). Given the unique composition and architecture, the hierarchical NiO/PANI nanoplate arrays show reversible multicolor changes, fast switching speeds of 90 and 120 ms for coloration and bleaching states, respectively, and a superior coloration efficiency of 121.6 $cm^2\ C^{-1}$ under a low voltage of 1.2 V. Additionally, the application of the NiO/PANI nanoplate array coated FTO glass causes a temperature difference of 7–7.6 °C under different ambient temperatures, making it very attractive for potential applications in energy-saving smart windows. Our strategy paves the way for the design and synthesis of hierarchical metal oxide/conducting polymer nanoarrays with enhanced properties for new applications.

Introduction

Hybrid organic/inorganic materials with new functionalities have become one of the most active research areas of materials science.[1,2] Nanohybridization of a conducting polymer and a metal oxide semiconductor has been recognized as one of the most attractive combinations for the organic/inorganic hybrids.[3,4] They often combine the elasticity and functionality of the former and the high thermal and chemical stability followed by the strength of the latter, thereby endowing them to be effective candidates in various applications, such as photovoltaics,[5–8] electrochemical capacitors,[9,10] transistors and electrochromic (EC) devices.[11–13] An EC device is one of the most promising technological applications of metal oxides and conducting polymers.[14] Although promising EC performances such as electrochemically stable and excellent switching reversibility have been demonstrated with metal oxide nanostructures, the coloration efficiencies and switching responses are still fall far behind that of conducting polymers.[13] Moreover, a conducting polymer is a unique class of conjugated polymers with interesting optical properties due to its multiple redox states accompanied by rich color changes, while the metal oxides often undergo single color changes.[14] Therefore, a synergistic combination of the merits of conducting polymers and metal oxides may provide an opportunity to develop a hybrid EC material with multicolor changing, high coloration

[a]State Key Laboratory for Modification of Chemical Fibers and Polymer Materials, College of Materials Science and Engineering, Donghua University, Shanghai 201620, P.R. China. E-mail: wanghz@dhu.edu.cn; Fax: +86-021-67792855; Tel: +86-021-67792881

[b]Engineering Research Center of Advanced Glasses Manufacturing Technology, Ministry of Education, College of Materials Science and Engineering, Donghua University, Shanghai 201620, P.R. China. E-mail: yaogang_li@dhu.edu.cn; Fax: +86-021-67792855; Tel: +86-021-67792526

[c]College of Chemistry, Chemical Engineering and Biotechnology, Donghua University, Shanghai 201620, China

[d]School of Materials Science and Engineering, Shanghai University, Shanghai 200444, P.R. China

† Electronic supplementary information (ESI) available: FESEM images of PANI films prepared using a potentiostatic procedure, galvanostatic procedure and potentiodynamic cycle, respectively; XRD patterns of porous NiO films prepared by the facile hydrothermal synthesis method; cyclic voltammetry curves of PANI films deposited by potentiostatic and galvanostatic procedures and a potentiodynamic cycle, respectively; transmittance spectra of PANI films and the corresponding digital photos of PANI films under different voltages; switching time characteristics measured at 632.8 nm between −0.6 and 0.8 V and ΔOD variation with respect to the charge density of the PANI films prepared by the potentiodynamic cycle; temperature dependence on time for NiO/PANI-1, NiO/PANI-2 and WO_3/PANI coated FTO glasses with the temperature of a thermostatic chamber fixed at 10 and 40 °C, respectively; peak current evolution of the WO_3/PANI and NiO/PANI-3 films during the step chronoamperometric cycles. See DOI: 10.1039/c4ta01722f

efficiency, fast switching response and outstanding device lifetime.

In the past decade, there have been continuous attempts to combine conducting polymers with metal oxides to form nanostructured hybrid EC materials.[15–19] A wide variety of nanocomposites of conducting polymers with metal oxides have been reported, such as PANI/WO_3,[20–22] PEDOT/TiO_2,[23] polypyrrole/WO_3,[24,25] and PANI/NiO,[26–28] where the organic and inorganic phases are held together by simple physical mixing. In this case, the interactions between the two phases are likely to be weak, because of the relatively small interfacial areas caused by oxide nanoparticle agglomeration.[29] Recently, covalently bonded PANI/TiO_2 and PANI/WO_3 hybrid thin films were fabricated using a sol–gel process or self-assembly technique to make interfacial interactions between the two components more prominent.[30,31] However, the hybrids showed compact structures, resulting in a relatively small surface area, which will influence the kinetics of coloration and bleaching processes that is controlled by ion diffusion. Moreover, the inorganic material covalently bonded with a conducting polymer has poor mechanical adhesion and electric connection with the supporting electrode, leading to slow transport of electrons into the EC layer to balance ions. Due to all of these drawbacks and limitations the advantages of each individual component in the nanocomposites cannot be fully exerted, and thus further development is required.

In an effort to overcome the above mentioned obstacles, the main challenge is to design and realize a system with large interfacial area and strong interfacial interactions, in which the organic and inorganic phases can work synergistically. In this respect, the following two issues should be taken into account. Firstly, with the hope of achieving a synergistic EC effect, the two components of the hybrid system should have a complementary or enhanced EC effect, such as WO_3/PANI or NiO/PANI. The former shows a dual-electrochromism effect due to the non-overlapping of the coloration and bleaching between PANI and WO_3, while a superimposed EC effect can be achieved for the latter because NiO and PANI possess synchronous coloration and bleaching voltages.[32,33] Secondly, the interconversion rate of conducting polymers between redox states is often limited by the slow transport of counter ions into the EC layer to balance charges, while the organized metal oxide nanostructures have a high surface-to-volume ratio and large tunnels for ion/electron intercalation processes.[34–36] Therefore, metal oxides can be served as host frameworks in the hybrid systems. By growing conducting polymers into such nanoarchitectures, hybrid assemblies with ordered structure and large interfacial area can be obtained. In such nanoscale configurations, both components have better electrical contact with the conductive substrate and will work synergistically.

In this article, we report a facile strategy for the construction of hierarchical metal oxide/conducting polymer hybrid assemblies with adjustable components and heterostructures on FTO glass substrates. Demonstrated examples include different nanostructures (nanorod arrays, nanorod-based networks and nanoplate arrays) of metal oxides (WO_3 and NiO) and PANI (nanostubs, nanoparticles and nano-wrinkles) with a hierarchical and porous morphology. This unique architecture holds the merits of high surface area and short diffusion distances for easy electrolyte penetration, leading to more efficient ion/electron transports, and thus the superior EC performances were expected. Additionally, a comparative study of the energy-saving effect of hierarchical nanocomposite coated FTO glass and non-coated FTO glass was also conducted with a model house. This is the first model house used for the practical evaluation of the solar-heat shielding ability of EC smart windows.

Results and discussion

We first present that the hierarchical WO_3/PANI hybrid can be obtained using combination of a hydrothermal process and electrochemical polymerization. It is worth noting that the morphologies of PANI were varied with the electropolymerization procedures (Fig. S1†). Fig. 1 shows the growth of WO_3/PANI nanoarrays on FTO glass substrates. The first step is to prepare a WO_3 nanorod array backbone by a hydrothermal method. Then PANI is directly assembled on the WO_3 nanorod surface by electrochemical polymerization.

The crystalline WO_3 film is composed of well-aligned rectangular WO_3 nanorods with a square cross-section of 80–120 nm (Fig. 2a and b). This unique nanostructure produces a coarse surface, which gives a larger surface area for the polymerization of PANI in the electrochemical processes. After carefully optimizing the potential cycling protocol at a scan rate of 100 mV s^{-1} for 100 cycles between −0.6 and 1.2 V, a thin PANI film is uniformly coated on each individual WO_3 nanorod, forming hierarchical WO_3/PANI nanoarrays (Fig. 2c and d). It can be seen from the inset of Fig. 2d that a PANI film has a nanostub-like morphology, which makes the surface of hybrid WO_3/PANI nanorods much rougher than the bare WO_3 nanorods and simultaneously the porous structure is well preserved.

The XRD patterns (Fig. 3a) reveal the crystalline WO_3 phase (hexagonal, JCPDS 85-2460) after electropolymerization; no obvious diffraction peaks of PANI are observed (Fig. S2†), and therefore we conducted FTIR (Fig. 3b) measurement to further check the components of the WO_3/PANI nanoarrays. For bare WO_3 nanorods, the strong peaks centered at 920 cm^{-1} (contributed from stretching vibrations of W=O bonds), 874, 830, and 764 cm^{-1} (corresponding to the stretching vibrations of O–W–O bonds) are observed.[37] For the WO_3/PANI nanoarrays, in addition to the peaks of WO_3 several characteristic peaks of PANI are noticed. Two bands at 1564 and 1496 cm^{-1} are due to the C=C stretching vibrations of a quinoid ring and a benzenoid ring (a quinoid ring and a benzenoid ring are the basic molecular units of PANI), respectively. The bands at 1295 and 1212 cm^{-1} belong to the C–N and C=N stretching mode, respectively.[38,39] In comparison with the FTIR spectra of pure PANI and WO_3, redshifts of the bands corresponding to the stretching vibrations of O–W–O bonds (from 874 to 868 cm^{-1}), C–N and C=N (from 1300 and 1243 cm^{-1} to 1295 and 1212 cm^{-1}, respectively) are found. This phenomenon indicates that the WO_3 phase is covalently bonded to PANI, which has been demonstrated in the previous literature.[31] Therefore, all results

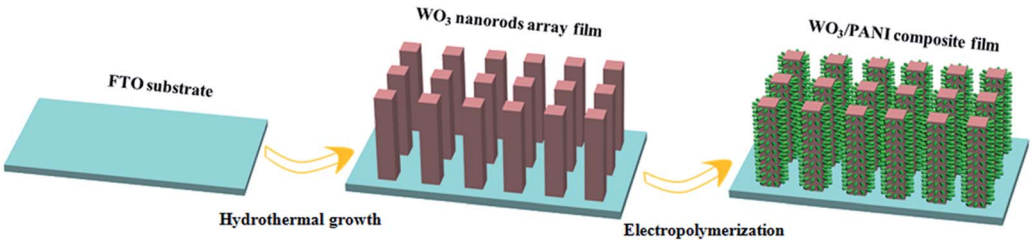

Fig. 1 Schematics of the fabrication of WO_3/PANI nanoarrays; the first step is to prepare a WO_3 nanorods array backbone by a hydrothermal method. Then PANI is directly assembled on the WO_3 nanorod surface by electrochemical polymerization.

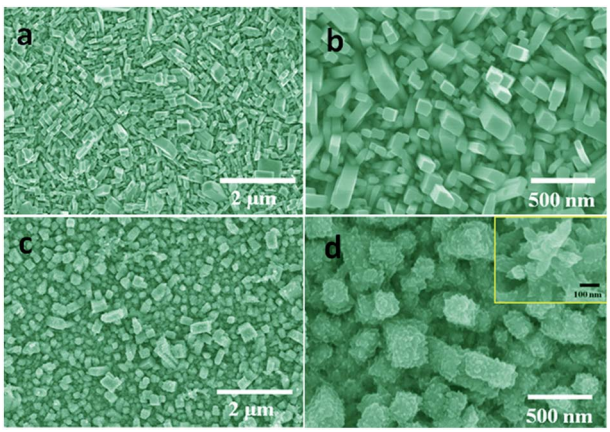

Fig. 2 (a and b) FESEM images of WO_3 nanorod arrays; (c and d) FESEM images of WO_3/PANI nanoarrays with a partially enlarged view in the inset of (d).

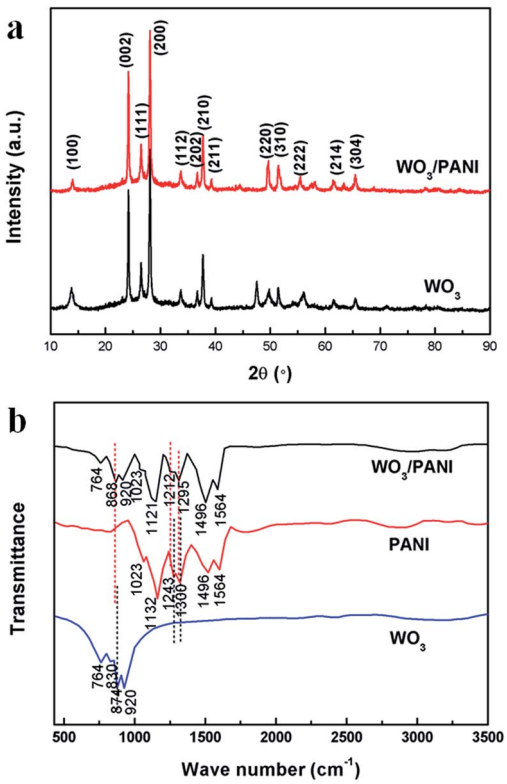

Fig. 3 (a) XRD patterns for both WO_3 and WO_3/PANI nanoarrays; (b) FTIR spectra of pure WO_3, PANI and hybrid WO_3/PANI nanoarrays.

are in complete agreement in showing the formation of hybrid WO_3/PANI nanoarrays.

Our strategy is powerful and general and can be easily extended to fabricate other metal oxide/conducting polymer hierarchical nanohybrids by simply choosing different metal oxide backbones (such as nanorods, nanoflakes, and nanoplates) and conducting polymers. To demonstrate the versatility, we have also fabricated three distinct types of NiO/PANI nanoscale configurations. Fig. 4 shows the result of the first type of NiO/PANI nanostructure (NiO/PANI-1) grown on FTO glass *via* similar polymer assembly of the NiO nano-network woven from nanorods. The nanorod diameter increases from 20 to 30 nm after homogeneous PANI nanoparticle growth, and the surface of hybrid NiO/PANI nanorods becomes much rougher than the bare NiO nanorods (Fig. 4c and d). Unfortunately, the PANI nanoparticles partially penetrated into the pores of the NiO backbone during the electrodeposition process, which is not conducive to the ion migration, and therefore may affect the EC properties.

For the second type of NiO/PANI nanostructure (NiO/PANI-2), a porous NiO nanoflake array is selected as the backbone for the subsequent electrodeposition of the PANI nanostructure (Fig. 5a–d). Unlike the first type, PANI nanorod-based networks are grown on the top surface of the NiO nanoflake (with a thickness of less than 10 nm and a width of about 2 to 3 μm) array. This is because both the NiO nanoflakes and open-pore voids between the nanoflakes are much larger than other NiO and WO_3 backbones in this study, and provide enough spaces for the growth of PANI nanorod networks. It is similar to the growth of PANI directly on FTO substrates, where the PANI nanorod networks are also grown (Fig. S1e and f†). Fig. 5e–h show the example of the obtained NiO/PANI nanoplate array (NiO/PANI-3). The third type of NiO/PANI nanoscale configuration holds the advantages of both NiO/PANI-1 and NiO/PANI-2. Firstly, each individual NiO nanoplate is covered with uniform PANI nano-wrinkles (the nanoplate thickness increases from 80 to 100 nm) and gives a coarse surface, which produces a larger active surface available for reactions in electrochemical processes. Secondly, the PANI nano-wrinkles are coated on the surface of NiO nanoplates and thus the porous structure is well preserved.

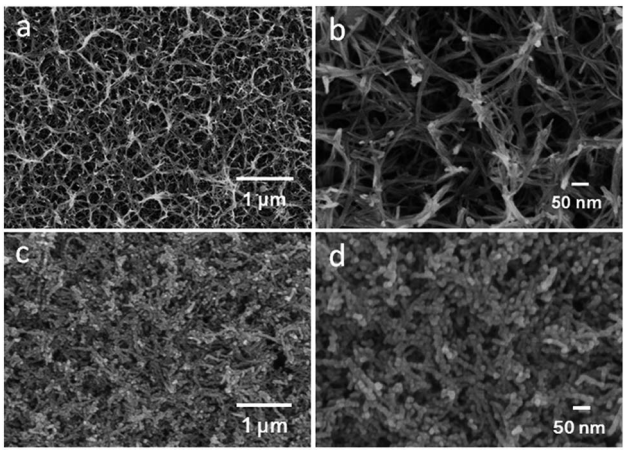

Fig. 4 (a and b) FESEM images of NiO nanorod-based networks; (c and d) FESEM images of the corresponding NiO/PANI nanohybrid composites.

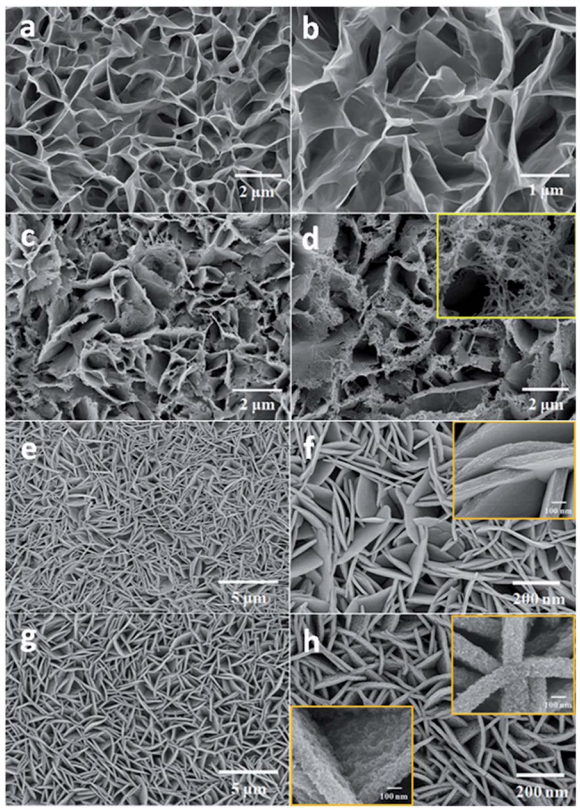

Fig. 5 (a and b) FESEM images of NiO nanoflakes and (c and d) the corresponding NiO/PANI nanohybrid composites; (e and f) FESEM images of NiO nanoplate arrays and (g and h) the corresponding NiO/PANI nanoarrays; the insets of (d), (f) and (h) show partially enlarged views.

The presence of PANI is also confirmed by the XRD patterns and FTIR spectra as shown in Fig. 6. From the XRD patterns, it is confirmed that the intensive diffraction peaks between 2θ ranges of 30–90° are indexed to a cubic NiO phase (JCPDS 04-0835, Fig. S3†), while the two broad peaks present at ~20 and

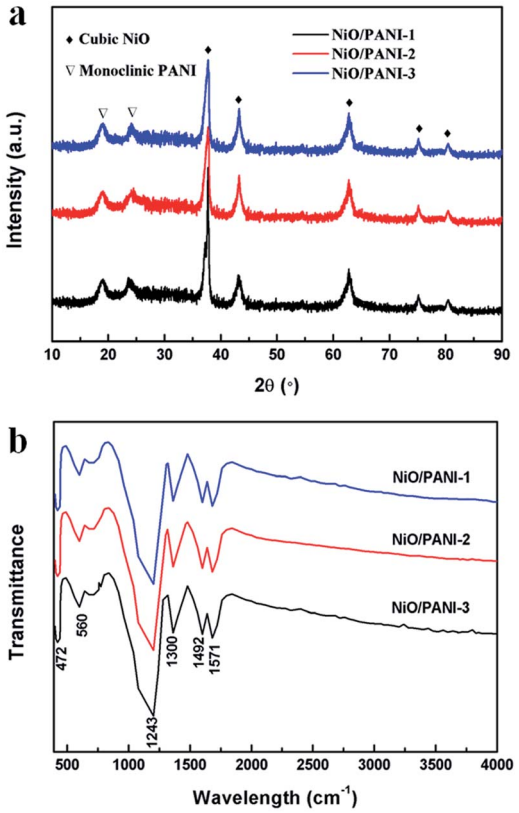

Fig. 6 (a) XRD patterns and (b) FTIR spectra for NiO/PANI-1, NiO/PANI-2 and NiO/PANI-3 nanohybrids, respectively.

25° are ascribed to the periodicity parallel and perpendicular to the polymer chain of PANI,[40] respectively, indicating the growth of crystalline PANI in the successive potential cycling protocol. From the FTIR spectra, it can be seen that the strong peaks centered at 472 and 560 cm^{-1} (attributed to stretching vibrations of Ni–O bonds) are observed;[41] in addition to the peaks of NiO the characteristic peaks of PANI are noticed. The results above are in complete agreement in showing the formation of hybrid NiO/PANI nanohybrids. Taking all, it is concluded that the developed methodology is general and powerful for preparing various metal oxide/conducting polymer nanoarchitectures with tunable heterostructures, components, and morphologies.

In view of the unique compositions and architectures, the as-prepared WO_3/PANI and NiO/PANI nanohybrids are anticipated to display promising applications in EC devices. Characterization of the electrochemical and EC properties of the WO_3/PANI nanorod arrays is shown in Fig. 7. The cyclic voltammetry (CV) curve of the WO_3/PANI nanorod arrays (Fig. 7a), as compared with those of pure WO_3 and PANI (Fig. S4†), has typical redox peaks of PANI (c_1/a_1, c_2/a_2 and c_3/a_3) and WO_3 (c_4/a_4), which indicates that a WO_3/PANI composite film is obtained successfully and it possesses activities of both PANI and WO_3. The redox couple c_4/a_4 is due to the WO_3-related redox process, involving the intercalation/deintercalation of Li^+ ions and electrons. The redox couples c_1/a_1 and c_3/a_3 correspond to the change between leucoemeraldine salt (LS) and emeraldine salt

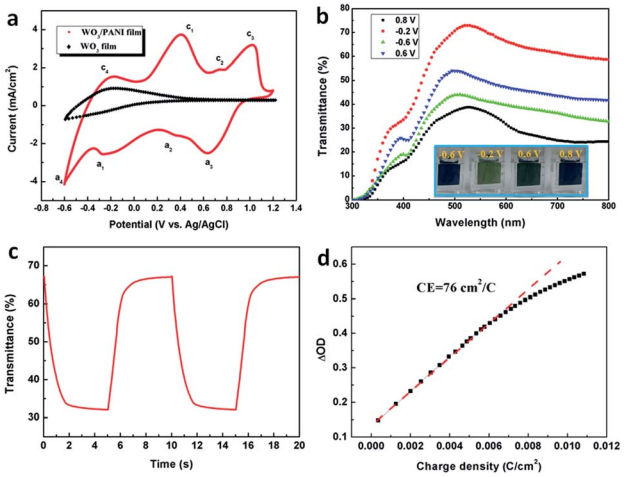

Fig. 7 (a) Cyclic voltammetry curves of pure WO_3 and WO_3/PANI nanoarrays measured in 1.0 M lithium perchlorate–PC solution with a sweep rate of 20 mV s^{-1} between −0.6 and 1.2 V; (b) transmittance spectra of WO_3/PANI nanoarrays under different voltages, with the inset showing the digital photos of WO_3/PANI nanoarrays under different voltages; (c) switching time characteristics for WO_3/PANI nanoarrays measured at 632.8 nm between −0.2 and 0.8 V; (d) ΔOD variation with respect to the charge density for WO_3/PANI nanoarrays.

(ES), emeraldine salt (ES) and pernigraniline salt (PS) of PANI with anion doping/dedoping processes, respectively, simply expressed as follows:[22]

$$\text{LS} \rightleftharpoons \text{ES}:$$
$$\underset{\text{light yellow}}{\text{PANI}} + 2n\text{ClO}_4^- \rightleftharpoons \underset{\text{green}}{(\text{PANI}^{2n+})(\text{ClO}_4^-)_{2n}} + 2ne^- \quad (1)$$

$$\text{ES} \rightleftharpoons \text{PS}:$$
$$\underset{\text{green}}{(\text{PANI}^{2n+})(\text{ClO}_4^-)_{2n}} + 2n\text{ClO}_4^- \rightleftharpoons \underset{\text{blue}}{(\text{PANI})^{4n+}(\text{ClO}_4^-)_{4n}} + 2ne^- \quad (2)$$

The redox couple c_2/a_2 can be ascribed to hydrolysis products of PANI due to over-oxidation at comparatively high potential.[42] The WO_3/PANI nanorod arrays show evident electrochromism with reversible multicolor changes under different applied potentials (inset of Fig. 7b) and the corresponding optical changes are recorded by the transmittance spectra (Fig. 7b). The optical modulation, *i.e.*, the transmittance variation of samples under different applied potentials, together with the switching speed and coloration efficiency are very important factors in practical applications of EC systems. For the WO_3/PANI nanorod arrays, the optical modulation is larger than that of a pure PANI film (Fig. S5†) and a maximum value of 42% is reached between −0.2 and 0.8 V at 632.8 nm. The chronoamperometry (by applying different potentials) and the corresponding *in situ* transmittance measurements were employed to study the switching time characteristics of the samples. In this case, the switching times were defined as the time required for a 90% change in the whole transmittance modulation. Fig. 7c shows the dynamic switching times of the WO_3/PANI nanorod arrays under a square wave voltage between −0.2 and 0.8 V with a pulse width of 5 s. The response times under the voltages of −0.2 and 0.8 V are found to be 500 and 800 ms, respectively,

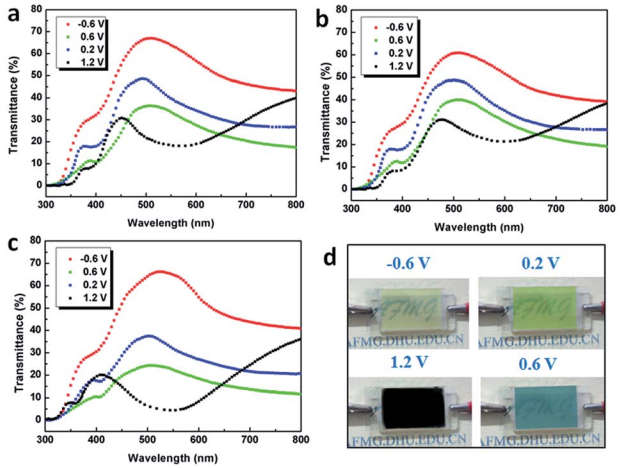

Fig. 8 (a–c) Transmittance spectra for NiO/PANI-1, NiO/PANI-2 and NiO/PANI-3 nanohybrids under different voltages, respectively; (d) digital photos of NiO/PANI-3 under different voltages.

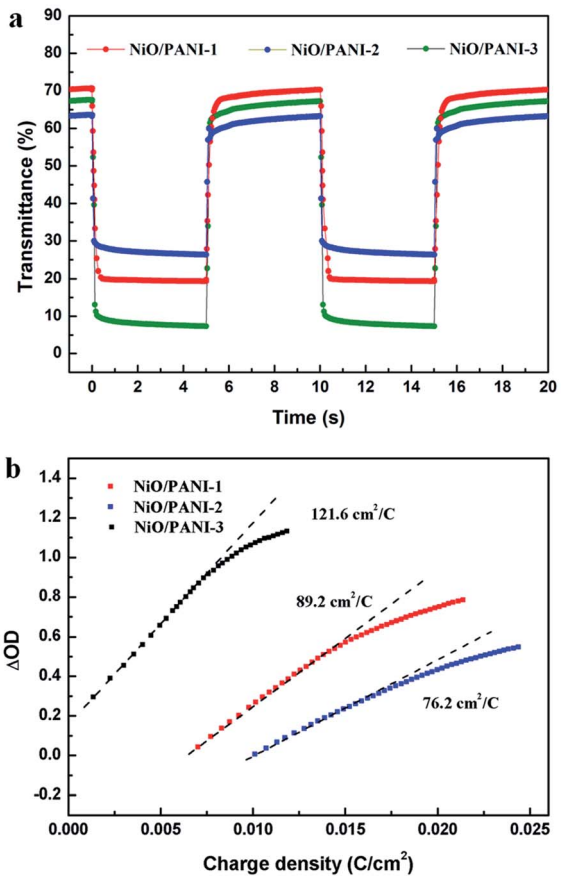

Fig. 9 (a) Switching time characteristics for NiO/PANI nanohybrids measured at 632.8 nm between −0.6 and 1.2 V; (d) ΔOD variation with respect to the charge density for NiO/PANI nanohybrids.

faster than those of the inorganic EC films such as WO_3 and NiO (more than 2 s),[34–36,43] PANI/WO_3 dense films (9.9 s),[22] and WO_3 nanorod embedded PANI composite films (0.9 s).[44]

Coloration efficiency (CE), namely the change in the optical density (ΔOD) per unit charge density (Q/A) during switching, is one of the most important criteria for selecting an EC material, and can be calculated according to the following formulae:

$$CE = \Delta OD/(Q/A) \quad (3)$$

$$\Delta OD = \log(T_b/T_c) \quad (4)$$

where T_b and T_c refer to the transmittances of the film in its bleached and colored states, respectively. Fig. 7d shows plots of the *in situ* ΔOD at 632.8 nm *versus* intercalation charge density (applying a voltage of 0.8 V) for the WO_3/PANI nanorod arrays. The CE is extracted as the slope of the line fitting the linear region of the curve. The calculated CE value of the WO_3/PANI nanorod arrays is 76 cm^2 C^{-1}. This value is much higher than that of the pure PANI film (Fig. S6†) (49.2 cm^2 C^{-1}), and shows an improvement of approximately 55%.

In comparison with the WO_3/PANI nanorod arrays, which shows the dual-electrochromism effect due to the non-overlapping of the coloration and bleaching between PANI and WO_3, a superimposed EC effect can be achieved for NiO/PANI hybrids because both the NiO and PANI show colored states at positive potentials and bleached states at negative potentials, respectively. Similarly, the NiO/PANI nanohybrids show evident electrochromism with reversible multicolor changes under different applied potentials (Fig. 8d). According to the above definitions, characterizations of the optical modulation, switching times and CE for the three types of NiO/PANI nanohybrids were conducted under different voltages with a pulse width of 5 s. Fig. 8a–c show the transmittance spectra of NiO/PANI-1, NiO/PANI-2 and NiO/PANI-3 nanohybrids under different voltages, respectively. As the applied potential increases from −0.6 to 1.2 V, the transmittance of the sample decreases sharply and thus large optical modulations of 50%, 38% and 62% are reached for NiO/PANI-1, NiO/PANI-2 and NiO/PANI-3 nanohybrids between −0.6 and 1.2 V at 550 nm, respectively. The maximum value of 62% is larger than those of the NiO/PANI dense film (31%)[45] and the porous NiO/PANI composite film (56%).[27]

The switching times of samples are calculated from Fig. 9a and summarized in Table 1. Obviously, the NiO/PANI-2 and NiO/PANI-3 show faster response speeds than NiO/PANI-1. The reason is that PANI nanoparticles partially penetrated into the pores of the NiO backbone during the electrodeposition process, which may hinder the ion migration rate. Fig. 9b shows plots of the *in situ* ΔOD at 550 nm *versus* intercalation charge density (applying a voltage of 1.2 V) for the NiO/PANI nanohybrids. As described in the previous section, NiO/PANI-3 holds the advantages of both NiO/PANI-1 and NiO/PANI-2. Thus, a high CE value of 121.6 cm^2 C^{-1} is achieved for NiO/PANI-3. This value is much higher than that of NiO/PANI-1 and NiO/PANI-2 (89.2 and 76.2 cm^2 C^{-1}, respectively), and shows an improvement of approximately 36–60%.

Table 1 Summary of the response times for the NiO/PANI hybrid films

Sample	Coloration times (1.2 V)	Bleaching times (−0.6 V)
NiO/PANI-1	384 ms	629 ms
NiO/PANI-2	63 ms	86 ms
NiO/PANI-3	90 ms	120 ms

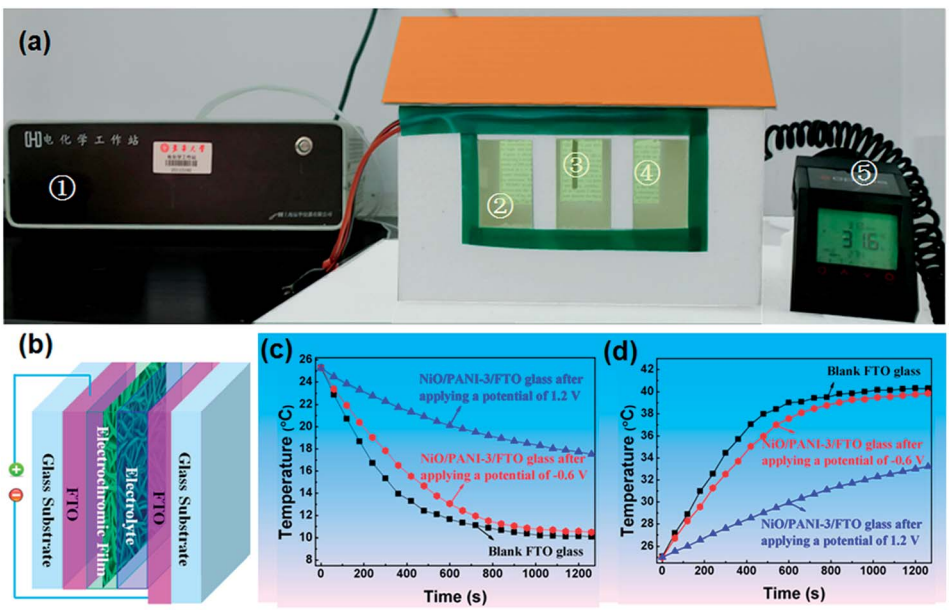

Fig. 10 (a) Photographic illustration of the testing system, (1) electrochemical workstation, (2 and 4) test windows installed in the front and back of the room, respectively, (3) temperature probe, and (5) portable thermometer; (b) the scheme of the test windows; (c) and (d) temperature dependence on time for NiO/PANI-3 coated FTO glass with the temperature of the thermostatic chamber fixed at 10 and 40 °C, respectively.

The noticeable EC performance of the hierarchical WO_3/PANI and NiO/PANI nanohybrids can be mainly attributed to the unique nanoarray architecture. On one hand, the WO_3 nanorod arrays and NiO nanoplate arrays with good adhesion to FTO substrates provide not only a stable mechanical support for the active PANI but also a template for homogeneous coverage of PANI, leading to large interfacial area and strong interfacial interactions, where the organic and inorganic phases can work synergistically. In addition, the large interfacial area will enhance the inter charge transfer and thus large optical contrast and fast switching speed can be achieved. On the other hand, the highly porous structure has a high surface-to-volume ratio that favors an efficient contact between active materials and the electrolyte. Meanwhile, the large tunnels formed by the ordered WO_3 and NiO nanostructures lead to a large diffusion coefficient, and reduce the diffusion path lengths for both electrons and ions, thus leading to fast switching kinetics.

The EC devices can be used in energy-saving smart windows to tune the indoor light and temperature. In this work, we have constructed a model house (Fig. 10a) to evaluate the solar-heat shielding ability of WO_3/PANI and NiO/PANI hybrid coated FTO glass; the results are shown in Fig. 10 and ESI.† The house was made of boards (thermal conductivity $k = 0.026\ Wm^{-1}\ K^{-1}$) with a thickness of 2.0 cm and the inner space had a volume of $1.8 \times 10^3\ cm^3$ ($22 \times 8 \times 10\ cm^3$). Six coated or non-coated FTO glasses were installed in the front and back of the room, respectively, and the space was sealed during the testing process. The experiment was performed at a thermostatic chamber and the temperature was fixed at 40 or 10 °C, while the initial temperature of the room was about 25 °C. A portable thermometer (laserSight LT, Optris, Germany) was employed to monitor the room temperature changes. The results (Fig. 10c) indicate that the application of the NiO/PANI-3 coated FTO glass causes a temperature difference of about 7.6 °C compared with the blank FTO glass, namely the inner room temperature can be maintained at 17.6 °C when the outer room (the thermostatic chamber) temperature fix at 10 °C. In another case, the inner room temperature can be maintained at 33 °C when the outer room temperature is fixed at 40 °C, therefore, a temperature reduction of about 7 °C is achieved. This property makes it possible to keep the inner room cool in summer and warm in winter.

Conclusions

In summary, we have demonstrated that the nanohybridization of the metal oxide and the conducting polymer can be achieved using combination of a hydrothermal process and electrochemical polymerization. Detailed experimental results reveal that PANI (nanostubs, nanoparticles and nanowrinkles) can directly assemble on different metal oxide nanostructures including WO_3 nanorod arrays and NiO nanorod networks, nanoflakes or nanoplate arrays. The morphology of PANI is dependent on the electropolymerization procedures (potentio-, galvanostatic and potential cycling protocols). Because of their unique composition and architecture, the hierarchical NiO/PANI nanoplate arrays show reversible multicolor changes, a fast switching speed of 90 and 120 ms for coloration and bleaching states, respectively, and a superior coloration efficiency of 121.6 $cm^2\ C^{-1}$ under a low voltage of 1.2 V. Moreover, the application of the NiO/PANI nanoplate array coated FTO glass causes a temperature difference of 7–7.6 °C under different ambient temperatures, making it very attractive for potential applications in energy-saving smart windows. Additionally, our powerful and general method could enable the fabrication of other metal oxide/conducting polymer heteronanostructures for selected applications in optical coating, electrochemical energy storage, and optoelectronic devices.

Experimental section

Preparation of WO_3 nanorod arrays and nanoporous NiO electrodes

Vertically aligned WO_3 nanorod arrays were grown on FTO coated glass substrates using a facile hydrothermal technique.[35] In a typical procedure, tungstenic acid (H_2WO_4) powder was dissolved in 30 wt% H_2O_2, while heating at 95 °C with stirring. The resulting solution was diluted using deionized water, giving a concentration of 0.1 M. The reaction solution for the hydrothermal use was obtained by mixing 10.5 mL H_2WO_4 solution (0.1 M), 3.5 mL HCl (3 M) and 1.2 mmol urea in 24 mL deionized water, and then transferred to a 70 mL Teflon-lined stainless steel autoclave, holding a vertically oriented WO_3 seed layer coated FTO glass. The WO_3 seed layer was deposited on FTO glass by spin-coating a seed solution of 1.5 g H_2WO_4 in 10 mL 30 wt% H_2O_2, followed by annealing at 400 °C for 1 h. Finally, the autoclave was sealed and maintained at 180 °C for 12 h. The samples were rinsed with deionized water several times and dried at room temperature.

The porous NiO nanostructures were prepared by another facile hydrothermal synthesis method as follows. Before hydrothermal growth, a seed layer was deposited on FTO glass *via* spin-coating a seed solution made by adding 0.5 g of nickel acetate to 9 mL of a mixed solution of ethanol and *n*-butanol with a volume ratio of 1 : 2, followed by heating at 60 °C in a vacuum oven for 6 h.

There are many factors affecting the formation and crystal growth of hydrothermal products, including the capping agent, solvent system, and reaction time. In our experiments, we note that using the same synthesis technique three distinct types of NiO nanostructures were obtained by modification of the reaction solution composition. For the NiO nanorod-based networks, 0.6 g of nickel acetate and 0.6 g of urea were added into 56 mL of deionized water. The reaction was kept at 180 °C for 6 h and then annealed at 400 °C for 2 h. For the NiO nanoflakes, 1.24 g of nickel acetate and 0.6 g of urea were added into 56 mL of absolute alcohol. The reaction was kept at 180 °C for 6 h and then annealed at 400 °C for 2 h. For the NiO nanoplate arrays, 0.6 g of nickel acetate, 0.3 g of potassium persulfate and 3 mL condensed aqueous ammonia were added into 53 mL of deionized water. The reaction was kept at 180 °C for 6 h and then annealed at 400 °C for 2 h.

Electrosynthesis of WO_3/PANI and NiO/PANI hierarchical hybrids

After a series of tentative experiments, the potentiodynamic methods were proven to be more appropriate for the deposition of PANI on the above WO_3 and NiO nanostructures than potentio- and galvanostatic procedures. The electrolyte for electro-polymerization of PANI was obtained by dissolving 0.93 g of aniline into 200 mL of 0.5 M H_2SO_4 solution. The polymerization of aniline was carried out by a simple, but careful optimization of a potential cycling protocol at a scan rate of 100 mV s^{-1} for 100 cycles between −0.6 and 1.2 V, where the above WO_3 nanorod array and nanoporous NiO electrodes as the working electrode, Ag/AgCl as the reference electrode and a Pt foil as the counter electrode. Finally, the samples were rinsed with deionized water and absolute alcohol, followed by heating at 60 °C in a vacuum oven for 6 h.

Characterization techniques

The morphology and microstructure of the samples were characterized by X-ray diffraction (XRD, D/max 2550 V, Rigaku, Japan, Cu Kα ($\lambda = 0.154$ nm) radiation at 40 kV and 200 mA in the 2θ range of 10–90°) and field emission scanning electron microscopy (FESEM, Hitachi, S-4800). The FTIR spectra were recorded using a Nicolet NEXUS-670 spectrometer from 500 to 3500 cm^{-1}. The *in situ* transmission spectra of the as-prepared electrodes in the colored and bleached states were measured over the range from 300 to 800 nm using a UV-vis spectrophotometer (Lambda 950, Perkin Elmer, Waltham, MA, USA).

Electrochemical and electrochromic measurements

The cyclic voltammetry (CV) measurements were carried out using an electrochemical workstation (CHI760D, Shanghai Chenhua Instruments, China) using a three-electrode test cell, which consisted of the working electrode (WO_3, NiO, WO_3/PANI or NiO/PANI), a platinum wire counter electrode, and a Ag/AgCl reference electrode in the electrolyte of 1.0 M lithium perchlorate ($LiClO_4$) in propylene carbonate (PC). The coloration/bleaching switching characteristics were recorded *in situ* using a UV-vis spectrophotometer with an absorbance wavelength of 632.8 and 550 nm for WO_3/PANI and NiO/PANI electrodes, respectively. The chronoamperometry tests were performed on the electrochemical workstation under different squarewave voltages with a pulse width of 5 s.

Energy-saving effect evaluation

The solar-heat shielding ability of WO_3/PANI and NiO/PANI hybrid coated FTO glass was conducted with a model house. The house was made of boards (thermal conductivity $k = 0.026$ Wm^{-1} K^{-1}) with a thickness of 2.0 cm and the inner space had a volume of 1.8×10^3 cm^3 ($22 \times 8 \times 10$ cm^3). Six coated or non-coated FTO glasses were installed in the front and back of the room, respectively, and the space was sealed during the testing process. The experiment was performed at a thermostatic chamber and the temperature was fixed at 40 or 10 °C, while the initial temperature of the room was about 25 °C. A portable thermometer (laserSight LT, Optris, Germany) was employed to monitor the room temperature changes.

Acknowledgements

We gratefully acknowledge the financial support by Natural Science Foundation of China (no. 51172042), Specialized Research Fund for the Doctoral Program of Higher Education (20110075130001), Science and Technology Commission of Shanghai Municipality (12nm0503900,13JC1400200), the Program for Professor of Special Appointment (Eastern Scholar) at Shanghai Institutions of Higher Learning, Innovative Research Team in University (IRT1221) and the Program of Introducing Talents of Discipline to Universities (no. 111-2-04).

Notes and references

1 C. Sanchez, P. Belleville, M. Popalld and L. Nicole, *Chem. Soc. Rev.*, 2011, **40**, 696.
2 M. J. Buehler, P. Rabu and A. Taubert, *Eur. J. Inorg. Chem.*, 2012, **32**, 5092.
3 G. H. Yu, X. Xie, L. J. Pan, Z. N. Bao and Y. Cui, *Nano Energy*, 2013, **2**, 213.
4 P. J. Hagrman, D. Hagrman and J. Zubieta, *Angew. Chem., Int. Ed.*, 1999, **38**, 2638.
5 M. Wright and A. Uddin, *Sol. Energy Mater. Sol. Cells*, 2012, **107**, 87.
6 S. D. Oosterhout, M. M. Wienk, S. S. van Bavel, R. Thiedmann, L. J. A. Koster, J. Gilot, J. Loos, V. Schmidt and R. A. J. Janssen, *Nat. Mater.*, 2009, **8**, 818.
7 W. R. Wei, M. L. Tsai, S. T. Ho, S. H. Tai, C. R. Ho, S. H. Tsai, C. W. Liu, R. J. Chung and J. H. He, *Nano Lett.*, 2013, **13**, 3658.
8 J. H. Heo, S. H. Im, J. H. Noh, T. N. Mandal, C. S. Lim, J. A. Chang, Y. H. Lee, H. J. Kim, A. Sarkar, M. K. Nazeeruddin, M. Grätzel and S. I. Seok, *Nat. Photonics*, 2013, **7**, 486.
9 L. Chen, Z. X. Song, G. C. Liu, J. S. Qiu, C. Yu, J. W. Qin, L. Ma, F. Q. Tian and W. Liu, *J. Phys. Chem. Solids*, 2013, **74**, 360.
10 K. R. Prasada and N. Miura, *Electrochem. Solid-State Lett.*, 2004, **7**, A425.
11 F. D. Franco, P. Bocchetta, C. Cali, M. Mosca, M. Santamaria and F. D. Quarto, *J. Electrochem. Soc.*, 2010, **158**, H50.
12 M. S. Hammer, C. Deibel, J. Pflaum and V. Dyakonov, *Org. Electron.*, 2010, **11**, 1569.
13 V. K. Thakur, G. Q. Ding, J. Ma, P. S. Lee and X. H. Lu, *Adv. Mater.*, 2012, **24**, 4071.
14 P. M. S. Monk, R. J. Mortimer and D. R. Rosseinsky, *Electrochromism and Electrochromic Devices*, Cambridge, New York, 2007.
15 W. Caseri, *J. Mater. Chem.*, 2010, **20**, 5582.
16 C. M. Amb, P. M. Beaujuge and J. R. Reynolds, *Adv. Mater.*, 2010, **22**, 724.
17 T. T. Steekler, X. Zhang, J. Hwang, R. Honeyager, S. Ohira, X. H. Zhang, A. Grant, S. Ellinger, S. A. Odom, D. Sweat, D. B. Tanner, A. G. Rinzler, S. Barlow, J. L. Bredas,

B. Kippelen, S. R. Marder and J. R. Reynolds, *J. Am. Chem. Soc.*, 2009, **131**, 2824.
18 S. Takagi, S. Makuta, A. Veamatahau, Y. Otsuka and Y. Tachibana, *J. Mater. Chem.*, 2012, **22**, 22181.
19 X. H. Xia, D. L. Chao, X. Y. Qi, Q. Q. Xiong, Y. Q. Zhang, J. P. Tu, H. Zhang and H. J. Fan, *Nano Lett.*, 2013, **13**, 4562.
20 P. K. Shen, H. T. Huang and A. C. C. Tseung, *J. Electrochem. Soc.*, 1992, **139**, 1840.
21 J. H. Zhu, S. Y. Wei, L. Zhang, Y. B. Mao, J. Ryu, A. B. Karki, D. P. Younge and Z. H. Guo, *J. Mater. Chem.*, 2011, **21**, 342.
22 H. G. Wei, X. R. Yan, S. J. Wu, Z. P. Luo, S. Y. Wei and Z. H. Guo, *J. Phys. Chem. C*, 2012, **116**, 25052.
23 L. J. Ma, Y. X. Li, X. F. Yu, Q. B. Yang and C. H. Noh, *Sol. Energy Mater. Sol. Cells*, 2008, **92**, 1253.
24 J. H. Zhu, S. Y. Wei, L. Zhang, Y. B. Mao, J. Ryu, P. Mavinakuli, A. B. Karki, D. P. Young and Z. H. Guo, *J. Phys. Chem. C*, 2010, **114**, 16335.
25 D. S. Lee, D. D. Lee, H. R. Hwang, J. H. Paik and J. S. Huh, *J. Mater. Sci.*, 2001, **12**, 41.
26 F. Svegl, A. S. Vuk, M. Hajzeri, L. S. Perse and B. Orel, *Sol. Energy Mater. Sol. Cells*, 2012, **99**, 14.
27 X. H. Xia, J. P. Tu, J. Zhang, X. L. Wang, W. K. Zhang and H. Huang, *Nanotechnology*, 2008, **19**, 465701.
28 M. Aleahmad, H. G. Taleghani and H. Eisazadeh, *Synth. Met.*, 2011, **161**, 990.
29 C. Janáky, N. R. de Tacconi, W. Chanmanee and K. Rajeshwar, *J. Phys. Chem. C*, 2012, **116**, 19145.
30 S. X. Xiong, S. L. Phua, B. S. Dunn, J. Ma and X. H. Lu, *Chem. Mater.*, 2010, **22**, 255.
31 J. Zhang, J. P. Tu, D. Zhang, Y. Q. Qiao, X. H. Xia, X. L. Wang and C. D. Gu, *J. Mater. Chem.*, 2011, **21**, 17316.
32 G. A. Niklasson and C. G. Granqvist, *J. Mater. Chem.*, 2007, **17**, 127.
33 G. F. Cai, J. P. Tu, D. Zhou, J. H. Zhang, X. L. Wang and C. D. Gu, *Sol. Energy Mater. Sol. Cells*, 2014, **122**, 51.
34 D. Y. Ma, H. Z. Wang, Q. H. Zhang and Y. G. Li, *J. Mater. Chem.*, 2012, **22**, 16633.
35 D. Y. Ma, G. Y. Shi, H. Z. Wang, Q. H. Zhang and Y. G. Li, *J. Mater. Chem. A*, 2013, **1**, 684.
36 D. Y. Ma, G. Y. Shi, H. Z. Wang, Q. H. Zhang and Y. G. Li, *Nanoscale*, 2013, **5**, 4808.
37 C. G. Granqvist, *Sol. Energy Mater. Sol. Cells*, 2000, **60**, 201.
38 A. Kellenberger, E. Dmitrieva and L. Dunsch, *J. Phys. Chem. B*, 2012, **116**, 4377.
39 W. A. El-Said, C. H. Yea, J. W. Choi and I. K. Kwon, *Thin Solid Films*, 2009, **518**, 661.
40 G. P. Song, J. Han and R. Guo, *Synth. Met.*, 2007, **157**, 170.
41 X. H. Xia, J. P. Tu, X. H. Xia, X. L. Wang and J. Y. Xiang, *Electrochem. Commun.*, 2008, **10**, 1288.
42 H. V. Hoang and R. Holze, *Chem. Mater.*, 2006, **18**, 1976.
43 J. Zhang, J. P. Tu, X. H. Xia, X. L. Wang and C. D. Gu, *J. Mater. Chem.*, 2011, **21**, 5492.
44 J. Zhang, J. P. Tu, G. H. Du, Z. M. Dong, Y. S. Wu, L. Chang, D. Xie, G. F. Cai and X. L. Wang, *Sol. Energy Mater. Sol. Cells*, 2013, **114**, 31.
45 A. C. Sonavane, A. I. Inamdar, H. P. Deshmukh and P. S. Patil, *J. Phys. D: Appl. Phys.*, 2010, **43**, 315102.